



Article

Decline in Planting Areas of Double-Season Rice by Half in Southern China over the Last Two Decades

Wenchao Zhu ¹, Xinqin Peng ¹, Mingjun Ding ² , Lanhui Li ^{1,*} , Yaqun Liu ³ , Wei Liu ¹, Mengdie Yang ¹, Xinxin Chen ¹, Jiale Cai ¹, Hanbing Huang ¹, Yinghan Dong ¹ and Jiaye Lu ¹

¹ School of Computer and Information Engineering, Xiamen University of Technology, Xiamen 361024, China; 2012001127@s.xmut.edu.cn (J.L.)

² School of Geography and Environment, Jiangxi Normal University, Nanchang 330028, China

³ Key Laboratory of Regional Sustainable Development Modeling, Institute of Geographic Sciences and Natural Resources Research, Chinese Academy of Sciences, Beijing 100101, China; liu yaqun@igsnr.ac.cn

* Correspondence: lilh@xmut.edu.cn

Abstract: Accurately tracking the changes in rice cropping intensity is a critical requirement for policymakers to formulate reasonable land-use policies. Southern China is a traditional region for rice multi-cropping, yet less is known about its spatial–temporal changes under the background of rapid urbanization in recent decades. Based on images from Landsat and MODIS and multiple land cover products, the gap-filling and Savitzky–Golay filter method (GF-SG), the enhanced pixel-based phenological features composite approach (Eppf-CM), random forest (RF), and the difference in NDVI approach (DNDVI) were combined to map the rice cropping pattern with a spatial resolution of 30 × 30 m over Southern China in 2000 and 2020 through Google Earth Engine (GEE). Subsequently, the spatial–temporal changes in rice cropping intensity and their driving factors were examined by Getis-Ord G_i^* and geographical detector. The results showed that the produced rice cropping pattern maps exhibited high accuracy, with kappa coefficients and overall accuracies exceeding 0.81 and 90%, respectively. Over the past two decades, the planting areas of double-season rice in Southern China decreased by 54.49%, and a reduction was observed across eight provinces, while only half of the provinces exhibited an increase in the planting areas of single-season rice. Compared to the year 2000, the planting area of the conversion from double- to single-season rice cropping systems in 2020 was 2.71 times larger than that of the conversion from single- to double-season rice cropping systems. The hotspots of the change in rice cropping intensity were mainly located in the central part of Southern China (excluding the Poyang Lake Plain). The decline in the rural labor force, coupled with ≥ 10 °C accumulated temperature and topographical factors, plays a crucial role in the decreased intensity of rice cropping. Our findings can be beneficial for realizing regional agricultural sustainability and food security.

Keywords: rice cropping intensity; accelerated decrease; rural labor force; Southern China; Google Earth Engine



Citation: Zhu, W.; Peng, X.; Ding, M.; Li, L.; Liu, Y.; Liu, W.; Yang, M.; Chen, X.; Cai, J.; Huang, H.; et al. Decline in Planting Areas of Double-Season Rice by Half in Southern China over the Last Two Decades. *Remote Sens.* **2024**, *16*, 440. <https://doi.org/10.3390/rs16030440>

Academic Editor: Peng Fu

Received: 3 December 2023

Revised: 16 January 2024

Accepted: 18 January 2024

Published: 23 January 2024



Copyright: © 2024 by the authors. Licensee MDPI, Basel, Switzerland. This article is an open access article distributed under the terms and conditions of the Creative Commons Attribution (CC BY) license (<https://creativecommons.org/licenses/by/4.0/>).

1. Introduction

Paddy rice covers over 9–11% of the world’s cropland [1] and is crucial for the livelihood of nearly half of the world’s population [2,3]. Rice cultivation significantly contributes to global food security and is essential in achieving the zero-hunger objective outlined in the United Nations’ Sustainable Development Goals (SDGs) by 2030 [4]. In China, the most populous country, rice is paramount for national food security [5]. Southern China is a traditional rice cultivation region and is a key area for developing multiple rice cropping systems [6], where increasing rice cropping intensity is seen as a key strategy for national food security. Nonetheless, challenges due to rapid urbanization and declining rural demographics have led to the phenomenon of conversion from double- to single-season rice cropping systems [7,8], abandonment of paddy fields [9], and thus a reduction in regional

grain production [10]. Therefore, accurately monitoring rice cropping intensity change in Southern China is a critical requirement for policymakers to formulate reasonable land-use strategies and thus guarantee regional food security.

Time-series remote sensing data are pivotal in the large-scale monitoring of rice growth, thereby tracking rice cropping intensity [11–13]. Medium- and lower-resolution optical remote sensing data, such as MODIS and AVHRR, have been widely employed for global and national mapping of rice paddies with resolutions between 0.25 and 8 km, mainly due to their advantages in temporal resolution [14–16]. However, due to small and fragmented crop fields and complex cropping systems in rice paddies [17,18], the mixed-pixel problem of these images is not conducive to accurately characterizing farming practices within heterogeneous landscapes [13], usually resulting in underestimation of the rice planting areas as compared to statistical data [19,20]. Higher spatial resolution imagery, such as from Landsat and Sentinel, has been acknowledged for improving the accuracy of mapping rice paddies [11,21]. Nonetheless, the time span of Sentinel images is short (from 2014 to the present), limiting long-term change analysis of rice cropping intensity [22,23], and cloud cover hampers the utility of long-term Landsat images at mid and low latitudes [15,24]. To harness the benefits of various datasets, several spatiotemporal fusion algorithms bridging the spatial resolution of Landsat and the temporal resolution of MODIS imagery have been developed [25], including the Spatiotemporal Adaptive Reflectance Fusion Model (STARFM) and its updated version—the Enhanced Spatiotemporal Adaptive Reflectance Fusion Model (ESTARFM) [26], as well as the recently proposed gap-filling and Savitzky–Golay filter method (GF-SG) [27]. Several studies have noted that the GF-SG method exhibits excellent performance in reconstructing continuous time-series vegetation index datasets [27–29]. The fusion algorithms provide opportunities to improve the accuracy of mapping multi-temporal rice paddies [30,31].

Phenology-based approaches, which capture key stages such as transplanting, heading, and harvesting through the incorporation of spectral indices and multi-resource data, have been widely applied to monitor rice planting areas [32,33]. Xiao et al. [32] proposed a method to identify rice paddies based on the differences between the water body index and vegetation index during the critical phenological stage of flooding required for rice transplanting. The phenology-based approaches have evolved from using a single key phenological period to multiple key phenological periods, employing richer spectral indices and auxiliary data, and have advanced from establishing one or more thresholds to combining machine learning techniques [30,34–36]. Ni et al. [36] proposed an enhanced pixel-based phenological features composite method (Eppf-CM) to address the issue of poor spectral separability between paddy rice and other crops using four distinctive phenological periods. They developed a paddy rice mapping method by integrating Eppf-CM and one-class support vector machine. Currently, this mapping method is primarily utilized in mid-latitude regions with a single rice-growing season, where it has proven to be effective. It should be noted that adapting the mapping method for low-latitude regions, characterized by cloudy weather and complex cropping systems, necessitates an abundant availability of high-quality temporal imagery [17,30,33,36].

Previous studies suggest a general decline in rice cropping intensity in Southern China [8,20,37]. These studies generally rely on medium- to low-resolution remote sensing images or a single remote sensing data source [38], leading to discrepancies in the findings across different regions. For example, Jiang et al. [8] reported that rice cropping intensity in the middle and lower reaches of the Yangtze River region has experienced the most significant decline, and Peng et al. [39] observed a significant shift from a double- to a single-season rice cropping system in Hunan Province from 2001 to 2007, with single-season rice reaching as much as 88% in the eastern part of Hunan by 2017 [22]. However, Li et al. [40] found that the change from a single- to a double-season rice cropping system was predominant in the plains of the middle reaches of the Yangtze River from 2003 to 2013, and Li et al. [41] also indicated a 20% increase in the rice cropping intensity across the Poyang Lake area from 2004 to 2010. Most current studies cover periods before 2015,

and there is little knowledge about the changes in rice cropping intensity in the southern regions over the past two decades. In addition, it remains unclear whether the significant migration of rural populations has a positive or negative effect on the changes in rice cropping intensity [7,8,19,42,43], and the interaction between changes in the rural labor force and other factors affecting the rice cropping intensity is still poorly understood.

In this study, our objective was to identify the spatiotemporal changes in rice cropping intensity and their associated driving factors over the past two decades in Southern China. Specifically, we developed a new strategy to map rice cropping intensity by integrating GF-SG filtering, Eppf-CM, random forest (RF), and the difference in NDVI (DNDVI) method. We then employed this strategy to map the distribution of rice cropping intensity in 2000 and 2020 with a 30 m spatial resolution through the Google Earth Engine (GEE) platform. Finally, we investigated the spatiotemporal changes in rice cropping intensity and explored the underlying mechanisms driving these changes.

2. Materials and Methods

2.1. Study Area

Southern China, located in a subtropical monsoon zone, is a typical region for double cropping of rice. The focus of this study spans the rice cultivation regions across eight provinces in Southern China: Guangdong, Guangxi, Fujian, Jiangxi, Hunan, Hubei, Zhejiang, and Anhui (Figure 1). Smallholders dominate the paddy rice agriculture, leading to a mixed agricultural landscape characterized by small-scale paddy fields. Due to differences in thermal conditions, Southern China can be roughly divided from north to south into areas of single-season and double-season rice cropping [8,44]. The early rice in the double-season cropping system is generally planted later in the northern regions compared to the southern regions, while the late rice is planted relatively earlier. The double-season rice cropping areas face a “rush-harvesting and rush-planting” period in late July to early August, which involves the harvesting of early rice and the planting of late rice, resulting in considerable pressure on rural labor. Over the past two decades, rapid urbanization and industrialization have led to a continual increase in the opportunity cost of rural labor and a rapid decline in the rural population [45], while per capita GDP has seen a steady rise [46]. These population and economic dynamics have profound implications for agricultural practices, particularly labor-intensive rice cultivation.

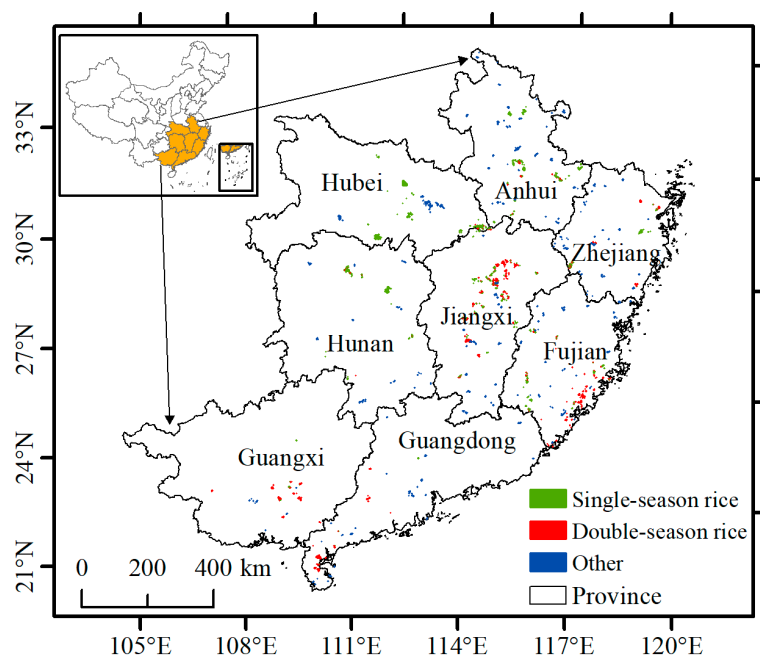


Figure 1. Study area and the distribution of the sample sites (region of interest, ROI).

2.2. Data Sources and Pre-Progress

2.2.1. Land Cover Datasets

The quality of the cropland distribution data is one of the keys to improving the accuracy of mapping rice paddies [38]. The availability of medium- to high-resolution land cover datasets for China (≤ 30 m) is on the rise. Yet, the accuracies of most datasets were around 80%, and relying on a single land cover product often fails to meet the needs for precise monitoring [47]. According to previous research, we use a fusion of multiple land cover datasets to reduce noise in the cropland layers [48]. This study selected four widely used land cover datasets, including the 30 m GLC data product (GlobeLand30) [49], the global 30 m land-cover classification with a fine classification system (GLC_FCS30) [50], the National Land Cover Dataset of China (NLCD-China) [51], and the China Land Cover Dataset (CLCD) [52] (Table 1). These data products all cover the years 2000 and 2020, and are primarily developed based on 30 m resolution remote sensing images, including the Landsat series TM5, ETM+, and OLI multispectral imagery. The datasets for 2020 also involve images from the HJ-1 satellite and GF-1 satellite imagery.

Table 1. Summary of four land cover datasets.

Name	Sources	Total Accuracy	Reference
GlobeLand30	www.globallandcover.com (accessed on 16 January 2024)	85.72% (2020)	Chen et al. [49]
GLC_FCS30	https://data.casearth.cn (accessed on 16 January 2024)	82.5%	Zhang et al. [50]
NLCD-China	https://www.resdc.cn/ (accessed on 16 January 2024)	—	Kuang et al. [51]
CLCD	https://zenodo.org/record/8176941 (accessed on 16 January 2024)	>79%	Yang et al. [52]

The fusion of cropland data involves three steps. Initially, cropland distribution layers are extracted from the four widely used land cover products. Subsequently, these cropland layers are converted to the WGS84 coordinate system. Upon this foundation, a spatial consistency analysis is conducted, and pixels with a consistency of three or more are identified as cultivated land. Finally, a new cropland distribution dataset for Southern China is created based on spatial consistency. It should be noted that these cropland distribution data are also utilized to minimize false positives [53].

2.2.2. Satellite Images and Vegetation Indices

All available images of surface reflectance from the Landsat 5 TM, Landsat 7 ETM+, and Landsat 8 OLI for two time frames (1999–2001 and 2019–2021) were acquired through the GEE platform. The challenge of acquiring high-quality Landsat imagery, exacerbated by a 16-day revisit cycle and persistent cloud cover during the southern monsoon season, often leads to a scarcity of usable data and gaps in temporal coverage. According to the methodologies of previous studies [30,36], we first utilized cloud-free pixels from all images within three-year intervals (1999–2001 and 2019–2021) to generate composite images rich in phenological information, thus mitigating the impact of cloud cover. Furthermore, the normalized difference vegetation index (NDVI) and the enhanced vegetation index (EVI) from the MODIS Vegetation Index products (MOD9A1) Version 6 were harnessed to reconstruct high-quality MODIS-Landsat NDVI and EVI time-series data using the GF-SG method, with more details provided in Section 2.3. Additionally, images from the Sentinel-2 MSI were employed as a supplementary source when validating the rice cropping intensity in 2020.

Integrating multi-dimensional spectral indices has proven more effective in revealing the characteristics of growth and development processes in various crops [54]. Therefore, based on reflectance data from Landsat images and MODIS, six spectral indices were

calculated in this study, including the bare soil index (BSI), land surface water index (LSWI), the green chlorophyll vegetation index (GCVI), NDVI, EVI, and plant senescence reflectance index (PSRI). Detailed calculation formulas for these spectral indices are presented in Table 2.

Table 2. Summary of six spectral indices and their expressions.

Indices	Calculation Formulas	Reference
BSI	$BSI = [(\rho_{swir} + \rho_{red}) - (\rho_{nir} + \rho_{blue})] / [(\rho_{swir} + \rho_{red}) + (\rho_{nir} + \rho_{blue})]$	Bera et al. [55]
LSWI	$LSWI = (\rho_{nir} - \rho_{swir}) / (\rho_{nir} + \rho_{swir})$	Xiao et al. [56]
GCVI	$GCVI = \rho_{nir} / \rho_{green} - 1$	Gitelson et al. [57]
NDVI	$NDVI = (\rho_{nir} - \rho_{red}) / (\rho_{nir} + \rho_{red})$	Tucker [58]
EVI	$EVI = 2.5 \times (\rho_{nir} - \rho_{red}) / (\rho_{nir} + 6 \times \rho_{red} + 7.5 \times \rho_{blue} + 1)$	Huete et al. [59]
PSRI	$PSRI = (\rho_{red} - \rho_{blue}) / \rho_{red_edge2}$	Merzlyak et al. [60]

2.2.3. Regions of Interest and Other Rice Cropping Pattern Datasets

For the collection of training and validation samples, field surveys combined with high-resolution historical imagery from Google Earth were employed. This method has been demonstrated to be both feasible and reliable for rice extraction and validation [8,22,61]. Rice cropping pattern samples were obtained in 2020 and 2021 through field research, resulting in 428 polygonal regions of interest (ROIs). We also integrated rice phenology information from the provincial farming database curated by the Ministry of Agriculture of China, along with findings from previous studies [8,30,37], to extract paddy rice ROIs through visual interpretation of Google Earth's high-resolution historical imagery according to the key phenological features. It is important to note that field sampling data were unavailable for the year 2000. We combined Google Earth's high-resolution historical images with NDVI time-series curves from Landsat 5 TM to generate paddy field ROI samples via visual interpretation. In total, 14,639 ROIs were obtained across the eight provinces, including 9884 paddy rice samples (with 6310 single-season rice samples and 3574 double-season rice samples, respectively) and 4755 non-paddy rice samples (Figure 1). These samples were randomly split into two sets with a 70:30 ratio, with the former serving as training samples for extracting rice planting intensity and the latter for validation and accuracy assessment.

In addition to the ROIs dataset, we utilized the high-resolution double-season rice mapping over Southern China from 2016 to 2020 by Pan et al. [23]. This pioneering dataset features one of the initial 10 m spatial resolution maps of double-season rice, constructed with Sentinel-1 imagery and an advanced time-weighted dynamic time-warping technique (hereafter referred to as TWDTW map). We adopted the TWDTW map as a complementary dataset for comparative analysis.

2.2.4. Statistical and Auxiliary Data

Topographical features, climatic variables, and socioeconomic variables were used to explore the underlying mechanisms of the changes in rice cropping intensity. Topographic data were sourced from the United States Geological Survey's global digital elevation model (DEM). Based on the DEM data, the elevation and slope of farmland were extracted. The ≥ 10 °C accumulated temperature was known as an indicator of the agricultural heat resource, and these data were obtained from the Resource and Environment Science Data Center of the Chinese Academy of Sciences (<https://www.resdc.cn> (accessed on 16 January 2024)). In addition, GDP and the proportion of the primary industry at the county level in 2000 and 2020 were acquired from the China County Statistical Yearbook (<https://www.stats.gov.cn> (accessed on 16 January 2024)). Census data at the county level for 2000 and 2020, including total population, male labor force, female labor force, agricultural labor force, and literacy rate among the population aged 15 and above, were derived from the China Population Census County Data (<https://www.stats.gov.cn> (accessed on 16 January 2024)).

2.3. Methods

2.3.1. Overview of the Rice Cropping Pattern Mapping Approach

This study maps high-precision rice cropping pattern intensity through the GEE platform. The research framework unfolds across four essential steps. Firstly, we reconstruct continuous high-quality MODIS-Landsat NDVI and EVI time-series data using the GF-SG method. Secondly, we map the planting area by combining the Eppf-CM and RF algorithms. Thirdly, we extract information on rice cropping patterns using a phenology-based DNDVI method. Finally, we validate the produced rice cropping patterns data, as shown in Figure 2.

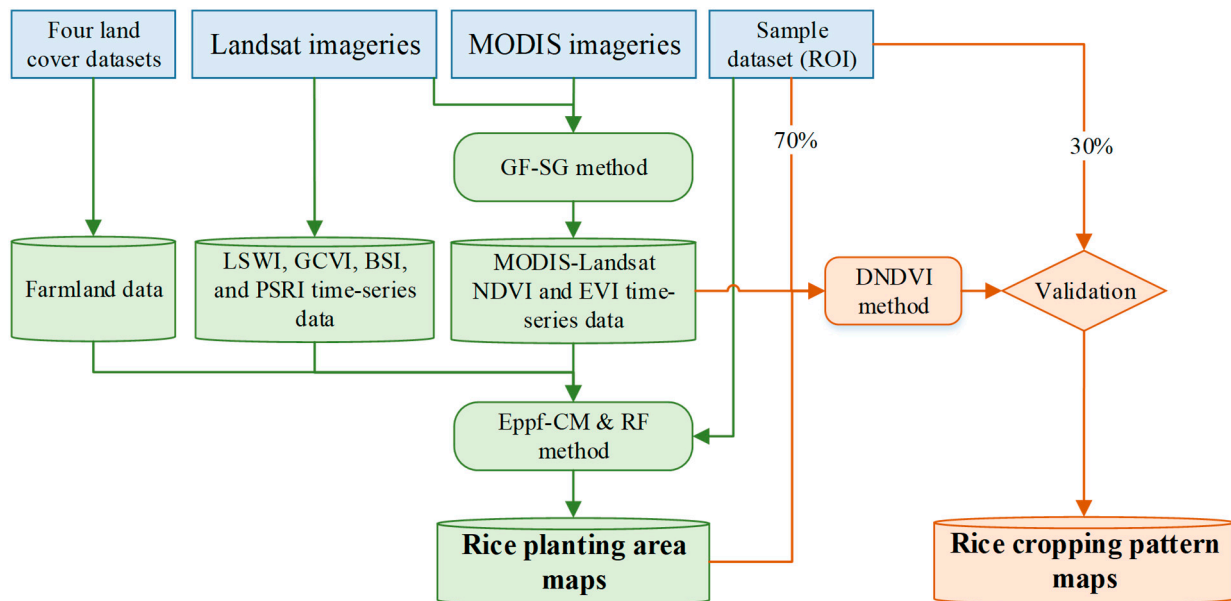


Figure 2. Flowchart illustrating the methods used for mapping the rice cropping patterns in Southern China.

2.3.2. GF-SG Method

The GF-SG method, proposed by Chen et al. [27], is widely used for reconstructing high-quality, continuous time-series datasets of vegetation indices, such as NDVI and EVI [28,29]. The GF-SG method involves two key steps. Initially, it fills the missing values in the original Landsat vegetation index time-series data by integrating the MODIS vegetation index time-series data and cloud-free Landsat vegetation index time-series data. Subsequently, it refines the composite vegetation index sequence to mitigate remaining noise through a weighted Savitzky–Golay filtering approach inherent to the GF-SG method. To process the large numbers of Landsat and MODIS images, the reconstruction in this study was conducted using the GF-SG method via the GEE platform. Specifically, the MODIS (MOD09Q1) images were fused with the original Landsat NDVI and EVI time series to generate a composite of 84 images across 40 periods for the year 2000 and 84 images over 46 periods for the year 2020, all at a 30 m spatial resolution and 8-day temporal resolution. For more details about the GF-SG method, see Chen et al. [27].

2.3.3. Rice Planting Area Mapping

This study combines the Eppf-CM with the RF classifier to accurately map rice planting areas. The Eppf-CM, developed by Ni et al. [36], enhances spectral distinguishability between paddy rice and other land covers. This method consists of two steps. Initially, it entails identifying four critical phenological periods—bare soil, transplanting, growth, and maturity—by analyzing time-series curves of the BSI, LSWI, GCVI, and PSRI. Subsequently, a new feature image is constructed by merging these four indices with EVI and NDVI, corresponding to the respective phenological period. However, when applying Eppf-CM to

multi-cropping rice areas in Southern China, adjustments to the key phenological periods are required [30,36]. By integrating the annual average time profiles of the four indices derived from Landsat and Sentinel images for different rice cropping patterns (Figure S1), we define the bare soil periods as DoY 90 to 120 and DoY 310–340; transplanting occurs from DoY 90 to 120 and from DoY 180 to 220; the growth period spans from DoY 180 to 220 and DoY 250 to 270; and maturity is defined as DoY 220–250 and DoY 280–310.

The RF algorithm, introduced by Breiman [62], is an ensemble learning method that refines the decision tree algorithm. RF is empirically more stable, accurate, and faster compared to many classical classifiers. Studies have increasingly recognized RF as an ideal method for extracting spatiotemporal information on crops such as paddy rice [35,63,64]. Its insensitivity to data noise and relative immunity to feature collinearity and redundancy are beneficial for mitigating the effects of noise in imagery from rainy seasons in Southern China, and accommodate the input of multiple key phenological period indicators. On the GEE platform, the RF method is directly invoked. To improve the generalizability of individual decision trees in RF to test data and prevent overfitting, the minimum size of terminal nodes (minLeafPopulation) was set to 10. Following the rules, and in conjunction with our new cropland distribution data, the rice paddies in Southern China were mapped for the years 2000 and 2020.

2.3.4. Rice Cropping Pattern Mapping

Based on the newly developed maps of rice paddies and high-quality NDVI time-series data reconstructed by the GF-SG algorithm, the phenology-based DNDVI method was further utilized to differentiate between single- and double-season rice [8]. The phenological periods of single- and double-season rice cause distinctive patterns in their annual NDVI curves, typically exhibiting unimodal and bimodal shapes, respectively, as depicted in Figure 3. Specifically, the NDVI of single-season rice shows an increasing trend from late May to early August, while that of double-season early rice decreases from late June to early August, resulting in contrasting NDVI trends. The NDVI of double-season early rice exhibits an increasing trend from the middle of August to late September, while that of single-season rice shows a decreasing trend. Additionally, from late September to early October, the NDVI of double-season late rice remains higher than that of single-season rice. The NDVI difference is calculated during specific time windows where the NDVI patterns of single- and double-season rice are notably distinct, as follows:

$$DNDVI = NDVI_{t_2} - NDVI_{t_1} \quad (1)$$

where $NDVI_{t_1}$ and $NDVI_{t_2}$ denote the NDVI values of images during the first and second half of a specific time window, respectively. $DNDVI$ represents the difference between $NDVI_{t_2}$ and $NDVI_{t_1}$. The $DNDVI$ values range between -2.0 and 2.0 . A $DNDVI$ value greater than 0 indicates an increasing NDVI phase, reflecting the growth period of paddy rice. Conversely, a decreasing NDVI trend indicates the maturation period of paddy rice. Based on the NDVI variation during the designated time window, a $DNDVI$ value below 0 in time window 1 (W1) suggests double-season early rice, whereas a $DNDVI$ value above 0 in time window 2 (W2) indicates double-season late rice. Conversely, the $DNDVI$ value above 0 in W1 and that below 0 in W2 denotes single-season rice [8].

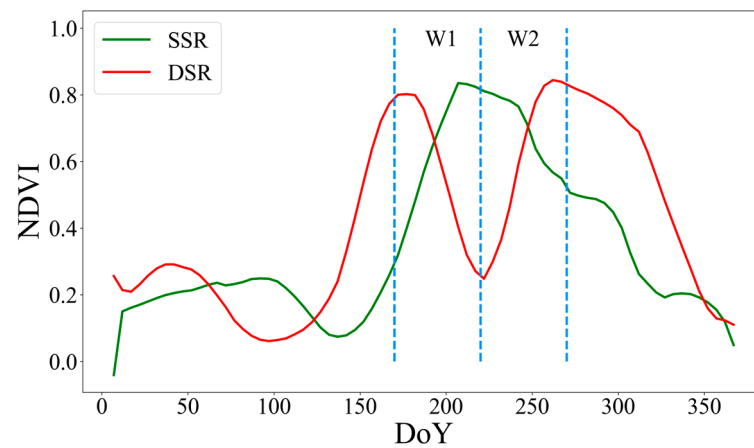


Figure 3. Temporal profiles of NDVI for single-season rice (SSR) and double-season rice (DSR), adopted from Jiang et al. [8].

2.3.5. Validation and Comparison

The accuracy of rice cropping pattern mapping was evaluated both at the pixel and the regional scales. Based on 30% ground validation of rice ROI, a confusion matrix was established by using four validation metrics, including the kappa coefficient, user's accuracy (UA), producer's accuracy (PA), and overall accuracy (OA). This confusion matrix is employed to verify the results of the rice planting area and cropping intensity mapping in Southern China.

In addition, we also compared our newly produced paddy rice cropping intensity maps with TWDTW maps developed by Pan et al. [23]. Subsequently, to compare the omission phenomenon between the two maps, the Sentinel-2 imagery and high-resolution historical imagery from Google Earth were employed as the reference map for visual interpretation.

2.3.6. Getis-Ord G_i^*

The Getis-Ord G_i^* model identifies statistically significant spatial clusters of high values (hotspots) and low values (cold spots) by calculating the Z-scores, p -values, and degree of clustering between blocks. The magnitude of the absolute Z-score indicates the intensity of clustering, with higher Z-values signifying more pronounced hotspots [65]. Generally, a p -value of less than 0.05 corresponds to a confidence level of 95%, defining statistical significance. In this study, we employ a confidence level above 95% to identify the spatial clustering characteristics of the change in the proportion of the planting areas of single-season rice.

2.3.7. GeoDetector Method

GeoDetector, an effective method for exploratory spatial data analysis proposed by Wang et al. [66], is not only capable of examining the spatial heterogeneity of a single variable but also detects the logical relationship between two variables. It has been widely applied in various natural and socio-economic fields [67,68]. This study employed this method to identify the dominant factors in rice cropping intensity changes in Southern China. The theory of this method is that if a particular factor shows significant spatial consistency with changes in rice cropping intensity, this indicates a decisive impact on these variations. The formula is expressed as follows:

$$q(r) = 1 - \frac{1}{N\sigma^2} \sum_{t=1}^G N_t \sigma_t^2 \quad (2)$$

where $q(r)$ represents the power of the influencing factor r on changes in rice cropping intensity. σ^2 is the overall regional variance, and σ_t^2 is the variance for category t of factor r . N_t and N denote the sample sizes for category t and the overall region, respectively. G is the number of categories of factor r . The value range of $q(r)$ is $[0, 1]$, with values closer to 1 indicating a greater impact of the factor on rice cropping intensity. The interaction detector could identify the interaction effect between two different factors r_1 and r_2 , which can be determined by the value of $q(r_1 \cap r_2)$. The interaction detector is used to identify the extent of interactions between different influencing factors, including the strength of these interactions and whether they are linear or nonlinear. If $q(r_1 \cap r_2) > q(r_1) + q(r_2)$, the variables nonlinearly enhance each other; if $\max(q(r_1), q(r_2)) < q(r_1 \cap r_2) < q(r_1) + q(r_2)$, the variables enhance each other. If $q(r_1 \cap r_2) < \min(q(r_1), q(r_2))$, the variables nonlinearly weaken each other; if $\min(q(r_1), q(r_2)) < q(r_1 \cap r_2) < \max(q(r_1), q(r_2))$, the variables unilaterally weaken each other.

3. Results

3.1. Spatial Patterns of Rice Cropping Intensity in Southern China

The planting areas of double-season rice are primarily concentrated in Guangdong and Guangxi provinces, and the central plains, such as Jiangnan Plain, Dongting Lake Plain, and Poyang Lake Plain (Figure 4). The planting areas of single-season and double-season rice exhibit prominent differences across eight provinces (Figure 4 and Table 3). In 2000, Guangxi Province led in double-season rice cultivation, followed by Guangdong Province, with areas of $450.24 \times 10^4 \text{ hm}^2$ and $381.72 \times 10^4 \text{ hm}^2$, respectively. Three provinces (Hunan, Jiangxi, and Hubei) exceeded $300 \times 10^4 \text{ hm}^2$. By 2020, Guangxi Province was the only province with more than $200 \times 10^4 \text{ hm}^2$ in double-season rice cultivation, with most provinces experiencing a reduction to half of that in 2000. Fujian, Jiangxi, Hunan, Hubei, and Anhui recorded an increase in single-season rice cultivation. These results suggest a general reduction trend in the planting areas of double-season rice across all provinces, with approximately half exhibiting an increased trend in the planting areas of single-season rice. In Southern China, the area planted with single-season rice was $878.70 \times 10^4 \text{ hm}^2$ in 2000 and $959.51 \times 10^4 \text{ hm}^2$ in 2020; double-season rice areas were $2282.94 \times 10^4 \text{ hm}^2$, $1038.94 \times 10^4 \text{ hm}^2$ for the same years. The findings indicate a slight increase, while the planting areas of double-season rice witnessed a rapid decrease, halving in size compared to the levels in 2000.

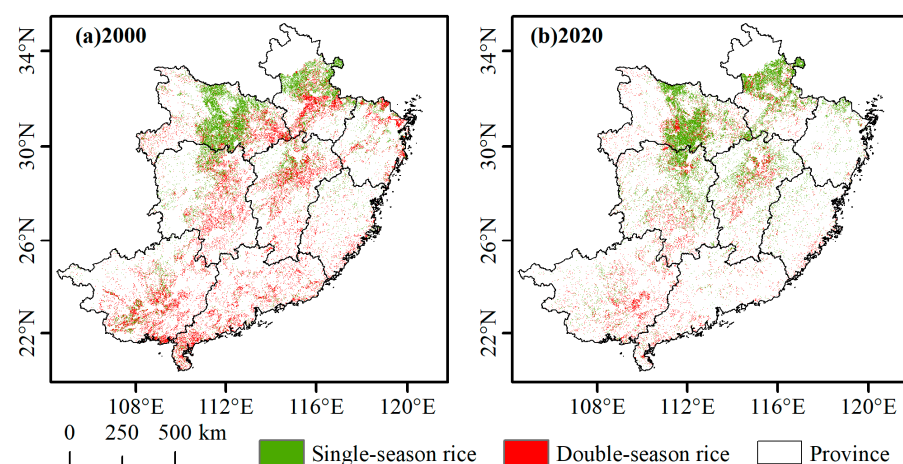


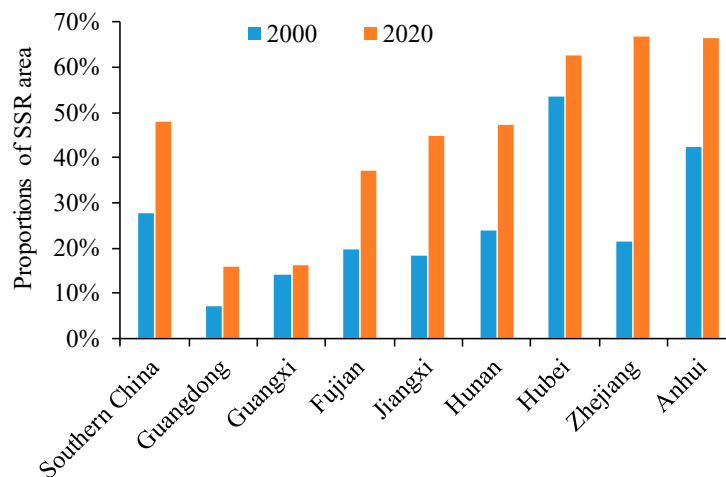
Figure 4. Spatial distribution characteristics of rice cropping systems in Southern China in 2000 (a) and 2020 (b).

Table 3. Summary of rice cropping intensity in Southern China.

Regions	2000		2020	
	SSR (10 ⁴ hm ²)	DSR (10 ⁴ hm ²)	SSR (10 ⁴ hm ²)	DSR (10 ⁴ hm ²)
Guangdong	29.08	381.72	17.50	94.24
Guangxi	73.57	450.24	45.50	234.08
Fujian	23.17	94.33	28.55	48.64
Jiangxi	71.24	317.65	120.16	147.66
Hunan	101.36	325.35	176.38	196.31
Hubei	350.49	302.78	311.20	186.52
Zhejiang	42.46	154.60	39.93	20.02
Anhui	187.34	256.27	220.29	111.47
Southern China	878.70	2282.94	959.51	1038.94

Note: SSR and DSR denote single-season rice and double-season rice, respectively.

In Southern China, the proportion of single-season rice was below 30% before 2000 but approached 50% by 2020 (Figure 5). At the provincial level, northern provinces notably had a higher proportion of single-season rice compared to southern provinces. In 2020, provinces with single-season rice exceeding 50% of the cultivation area included Hubei, Zhejiang, and Anhui, with Jiangxi and Hunan close to 50%. At the county level, the proportion of counties with over 50% single-season rice cultivation was 20.27% and 37.47% in 2000 and 2020, respectively (Figure S2), and in the latter case, they were primarily located in western Hunan Province, central Hubei Province, central-western Zhejiang Province, and northern Anhui province.

**Figure 5.** The proportion of the planting areas of single-season rice (SSR) at the provincial level in Southern China in 2000 and 2020.

3.2. Accuracy Assessment

The rice cropping pattern maps generated for Southern China exhibited high accuracies overall, with kappa coefficients of 0.81 in 2000 and 0.85 in 2020. The overall accuracies (OAs) for these years were 90.67% and 95.68%, respectively, as shown in Table 4. Both user's and producer's accuracies surpassed 87% for each year. A temporal analysis revealed a slight increase in classification accuracy for 2020 compared to 2000. Spatially, the classification accuracies in northern provinces, such as Hubei, Zhejiang, and Anhui, were higher than those in southern provinces, including Guangdong, Guangxi, and Fujian. This discrepancy is attributed to the more prevalent cloud cover, as well as the more intricate cropping systems in southern provinces. Across most provinces, kappa coefficients and overall accuracies for paddy rice cropping pattern classification exceeded 0.8 and 90%, respectively. In the years 2000 and 2020, the lowest kappa coefficients were observed in

Fujian and Guangxi, yet even the lowest kappa coefficients and overall accuracies were above 0.75 and 87%, respectively.

To further validate the accuracy of our newly developed rice cropping pattern maps, four representative regions were selected for comparative analysis with the TWDTW rice maps. Overall, the patterns of our new double-season rice map are generally consistent with the early-season rice of TWDTW (Figure 6). However, upon cross-referencing our new rice cropping pattern maps with historical high-resolution images, we observed superior comprehensive coverage and fidelity as compared to TWDTW maps. Specifically, our identified double-season rice fields minimize the presence of tiny holes within them and reduce the number of missing classifications for this crop. Additionally, our maps circumvented the misclassification of lotus ponds and roadside greenery as rice paddies.

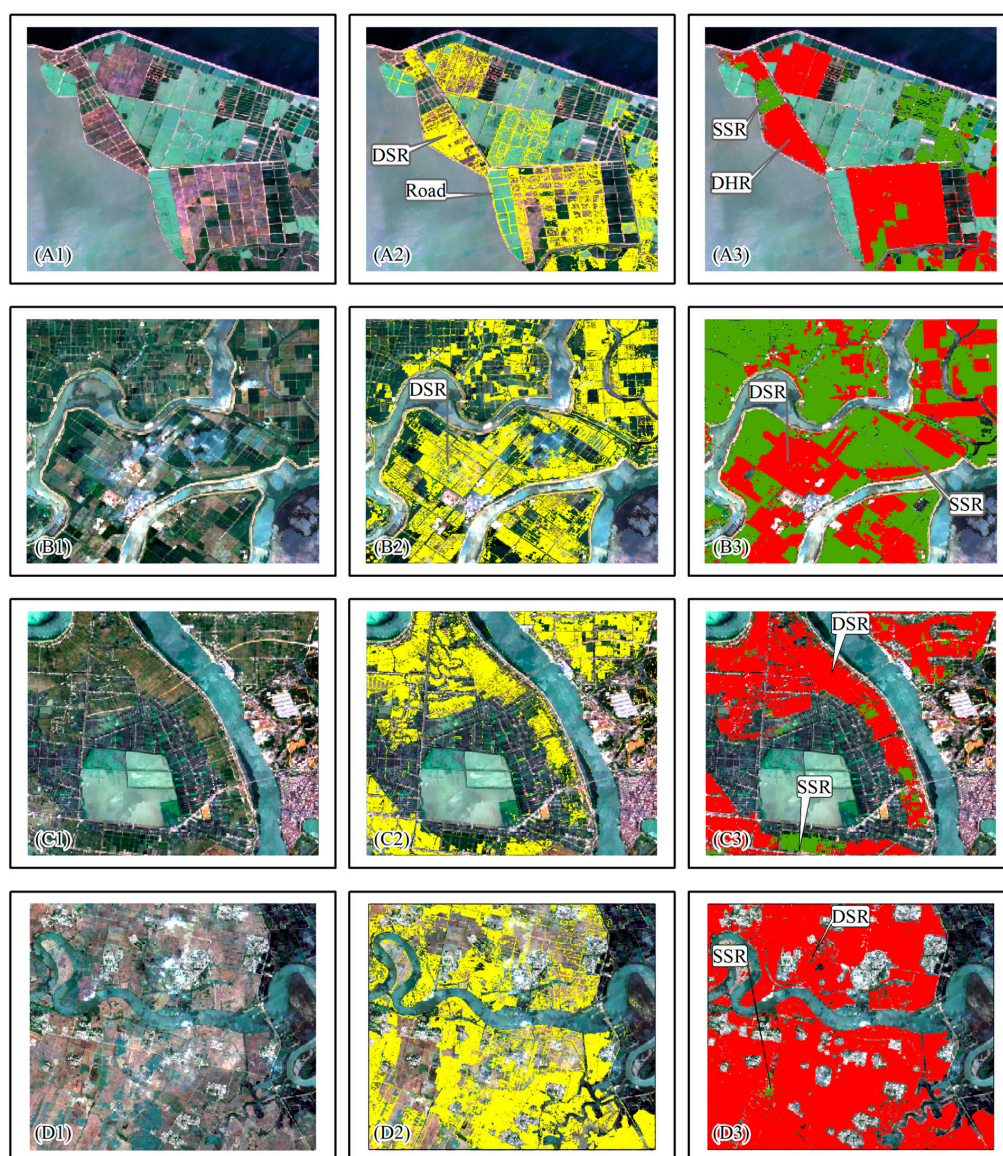


Figure 6. Comparison between our new rice cropping pattern maps and TWDTW maps. (A–D) The areas in Yugan County in Jiangxi Province, Xinjian County in Jiangxi Province, Jiuluo County in Hunan Province, and Leizhou County in Guangdong Province, respectively. (1–3) The original Sentinel-2 imagery on 12 July 2020, the TWDTW double-season early rice map (yellow) as documented by Pan et al. [23], and our new map with single-season rice depicted in green and double-season rice in red, respectively.

Table 4. Summary of accuracy assessment of rice cropping pattern mapping.

Region	2000				2020			
	Kappa	OA (%)	UA (%)	PA (%)	Kappa	OA (%)	UA (%)	PA (%)
Southern China	0.81	90.67	93.55	87.69	0.85	95.68	91.95	94.82
Guangdong	0.78	89.45	96.47	82.00	0.89	98.76	83.44	96.58
Guangxi	0.78	89.37	93.39	85.32	0.83	94.78	82.73	89.74
Fujian	0.75	87.73	91.91	83.48	0.84	91.82	88.94	93.27
Jiangxi	0.81	90.77	93.68	87.25	0.87	94.15	90.48	91.25
Hunan	0.83	91.79	92.78	90.90	0.84	96.1	98.63	96.83
Hubei	0.83	91.91	90.38	94.00	0.91	98.41	99.80	98.54
Zhejiang	0.84	92.34	97.74	86.59	0.91	95.82	94.06	95.05
Anhui	0.84	92.01	92.03	92.01	0.84	95.63	97.54	97.32

Note: OA, UA, and PA denote overall accuracies, user's accuracies, and producer's accuracies, respectively.

The above assessments indicate that the rice cropping pattern maps developed for Southern China—utilizing a combination of GF-SG filtering, Eppf-CM, random forest, and DNDVI—are reliable. This provides a data foundation for subsequent analyses of the changes in rice cropping intensity and their underlying mechanisms in Southern China.

3.3. Spatial–Temporal Change in Rice Cropping Intensity in Southern China

Compared to the year 2000, the planting areas in Southern China that shifted from double- to single-season rice in 2020 were 2.71 times larger than those that shifted from single- to double-season rice (Figure 7a). The former are predominantly located in the Poyang Lake and Dongting Lake Plain, as well as southern Anhui, while the latter are mainly concentrated in the center of Hubei Province and south of Anhui Province. In Southern China, the change in the proportion of the planting areas of single-season rice shows significant regional differences (Figure 7b). Compared to 2000, two-thirds of the counties in 2020 experienced an increase in the proportion of planting areas of single-season rice, with half of these counties experiencing an increase of more than 10%. Spatially, these changes were primarily concentrated in the center of the study area (Figure 7b). In summary, over the past two decades, there has been an overall decrease in rice cropping intensity observed across Southern China.

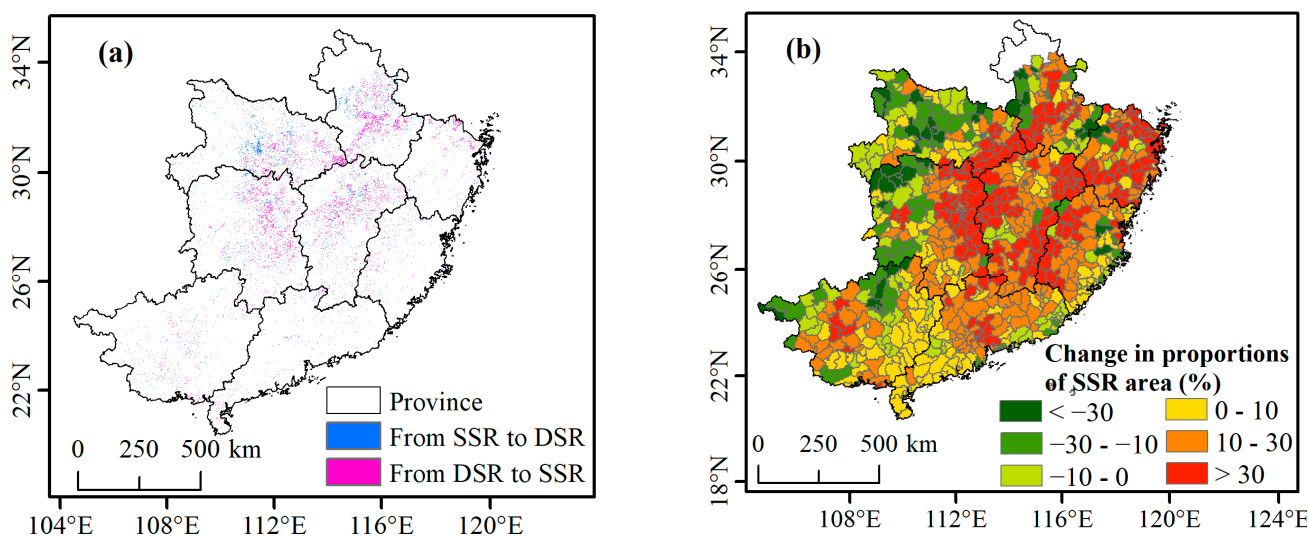


Figure 7. Spatial pattern of the change in the rice cropping pattern (a) and in the proportion of planting areas of single-season rice at the county level (b) in Southern China from 2000 to 2020.

Using Getis-Ord G_i^* analysis, it was revealed that, compared to 2000, the hotspots of the change in the proportion of the planting areas of single-season rice in 2020 were mainly located in the central part of Southern China (excluding the Poyang Lake Plain) and most of Zhejiang Province (Figure 8). The cold spots of the change in 2020 were primarily in western Hunan Province, western Hubei Province, northeastern Guangxi Province, and eastern Fujian Province.

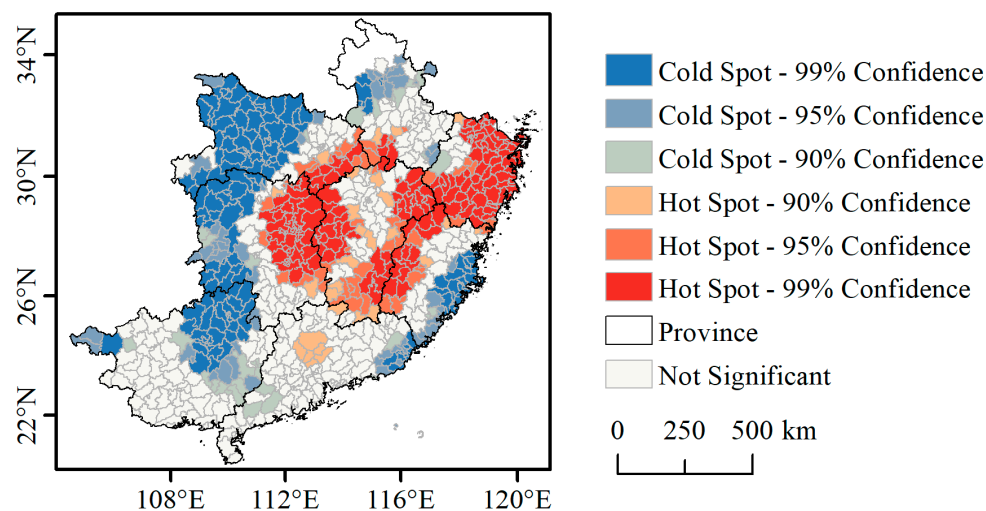


Figure 8. Hotspot analysis map of the proportion change in planting areas of single-season rice in Southern China from 2000 to 2020.

3.4. Driving Factors of the Changes in Rice Cropping Intensity

This study employed a geographical detector to analyze the impact of topographical features, climatic variables, and socioeconomic variables on the changes in rice cropping intensity from 2000 to 2020. The results showed that changes in the agricultural labor force, ≥ 10 °C accumulated temperature, and slope of farmland were the top three factors influencing rice cropping intensity changes, contributing 18%, 18%, and 17%, respectively (Figure 9a). Rice cultivation, a labor-intensive agricultural activity, has been significantly impacted by rapid urbanization and industrialization. These processes have led to a rapid decrease in the rural population and an increase in opportunity costs for farm labor, resulting in a shortage of agricultural labor and rising labor wages. This shortage has resulted in a widespread transformation from double- to single rice cropping systems or even abandonment of farmlands, consequently reducing rice cropping intensity. The ≥ 10 °C accumulated temperature decreases with increasing latitude, partially explaining why provinces like Hubei Province and Anhui Province in the north have a faster increase in the proportion of planting areas of single-season rice compared to southern provinces like Guangdong Province and Guangxi Province. The slope of farmland is the second most significant natural factor. In areas with steeper slopes, farmers face challenges in implementing mechanized operations, which in turn impacts the rice cropping intensity. The change in the male labor force had an 11% explanatory power for the change in rice cropping intensity, significantly higher than female labor force changes, indicating a greater impact of male labor migration on rice cropping intensity. Furthermore, changes in GDP also had a 10% explanatory power, exceeding the impact of the change in the proportion of the primary industry.

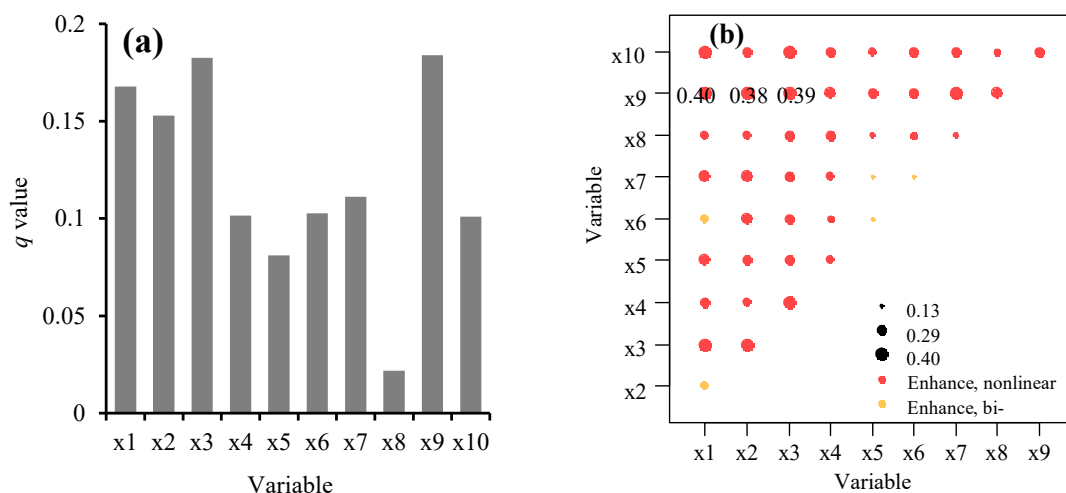


Figure 9. Impact of various environmental factors on the changes in rice cropping intensity. x1–x10 represent slope, elevation, ≥ 10 °C accumulated temperature, GDP change, change in the proportion of the primary industry, total population change, male labor force change, female labor force change, agricultural labor force change, and literacy rate change among the population aged 15 and above, respectively.

The interactions between farmland resources, climatic factors, economic shifts, and labor force changes predominantly exhibited a nonlinear enhancing relationship with rice cropping intensity (Figure 9b). The interaction between changes in the agricultural labor force and the slope of farmland, along with the interaction with elevation, accounted for 40% and 38% respectively. This suggests that in mountainous areas with medium- and low-quality cropland, agricultural labor scarcity is a key factor in the reduction in rice cropping intensity, as evidenced by cropland abandonment and a shift to non-grain crops. The interaction between labor force changes and ≥ 10 °C accumulated temperature had a 39% explanatory power, indicating that northern provinces (e.g., Hunan, Hubei, and Anhui) have low accumulated temperature with a short time window of “rush-harvesting and rush-planting”, requiring more agricultural labor compared to southern provinces. This labor decline, especially in the male workforce, has led to a large-scale transformation from a double- to single-season rice cropping system in a typical region with double cropping of rice in the areas along the Yangtze River (Figure 4). Additionally, the interaction between changes in the agricultural labor force and GDP changes had an explanatory power of 0.33. In summary, in the context of economic development, the reduction in the rural labor force, coupled with topographical and climatic factors, plays a crucial role in the decrease in rice cropping intensity in Southern China.

4. Discussion

This study developed a new strategy to map rice cropping intensity by integrating GF-SG filtering, Eppf-CM, RF, and the DNDVI method, which was then employed to map rice cropping intensity in 2000 and 2020 with a 30 m spatial resolution through the GEE platform. The new maps achieved overall accuracies of 90.67% and 95.68% for the respective years, which can be attributed to the following three factors: Firstly, multi-temporal and high-quality NDVI time-series data were reconstructed using the GF-SG algorithm, which can offset the impact of cloud contamination on rice mapping in Southern China to some extent [30]. Utilizing multi-temporal satellite imagery has proven to be more robust than using a single image for mapping rice planting areas [69]. Secondly, we adopted Eppf-CM with more spectral parameters in four rice phenological periods to reduce the uncertainties of rice plating area mapping in Southern China with complex cropping systems. Eppf-CM using four rice phenological periods with six spectral indexes could characterize the spectral characteristics in paddy rice lifespan and improve the spectral separability between rice

and other land cover types (e.g., wetlands and swamps) [36]. Combining with Eppf-CM and RF classifier might produce higher overall accuracies of rice planting area mapping than when used separately. Additionally, this study integrated four existing farmland datasets to reduce the misidentification of other types of land as rice fields (Figure S3). Furthermore, the high-precision rice maps benefit in improving the accuracy of rice cropping pattern maps [8]. Based on the newly developed maps of rice paddies and high-quality NDVI time-series data, we extracted cropping intensity information using a phenology-based DNDVI method. Previous studies noted that the identified rice paddies were generally accompanied by some tiny holes within them [23,70], and our strategy effectively reduced this phenomenon to some extent (Figure 6). In summary, our strategy allowed for the integration of multi-temporal satellite imagery and multiple phenological periods to identify rice cropping patterns, which might advance the phenology-based agricultural remote sensing mapping method in Southern China, even in low-latitude regions.

The double-season rice planting areas witnessed an overall rapid decrease over the past two decades, which is in agreement with previous studies [8,20,37]. Our results showed that the planting areas of double-season rice have decreased by more than half during the past two decades, while Qiu et al. [20] tracked the changes in rice cropping intensity using MODIS imagery, and they pointed out a more pronounced decline during 2000–2013. The differences can be attributed to the use of higher-resolution data and a combination algorithm in our study, enabling the detection of a greater number of fragmented rice paddies. In addition, our results show that the proportion of single-season rice increased by 27% in Jiangxi Province over the past two decades, while Gan et al. [71] noted that the proportion of planting areas of single-season rice increased by more than 10% during 2018–2021, which suggests that the declining trend might be accelerating. We also found that only half of the provinces exhibited an increased trend in the planting areas of single-season rice, which might be related to the occupation of farmland by construction sites [51], the non-grainification of farmland [72], and farmland abandonment [73].

A reduced rural labor supply due to urbanization and economic growth, alongside topographical and thermal factors, plays a crucial role in the decreasing rice cropping intensity in Southern China. High labor requirements and other associated costs make rice production less attractive to farmers in some regions [5], especially for the areas with a short time window of “rush-harvesting and rush-planting” and hilly regions [74]. In the context of comprehensive poverty alleviation, with the deepening implementation of rural industry revitalization and rural land management rights transfer policies, the patterns of farmland cultivation are likely to undergo further changes [75]. Given the ongoing urbanization, the rise in labor wages, and the aging population trend, it is expected that the decline in rice cropping intensity will continue in the future [8]. Therefore, it is imperative for governments to continue developing high-standard farmland and enhancing mechanization levels to compensate for the shortage of agricultural labor in traditional double-season rice cultivation plains, particularly in areas with a period of “rush-harvesting and rush-planting”. Additionally, governments should persist in providing incentives for agricultural practitioners and implement policies to prevent non-grainification of farmland, thus ensuring national food security.

Although the accuracy of rice cropping pattern mapping has improved, this study did not account for the black swan event in the spring of 2020—the COVID-19 pandemic—which might introduce uncertainties into the results regarding changes in rice cropping intensity between 2000 and 2020, particularly for Hubei Province. Additionally, although we used GF-SG to construct high temporal and spatial resolution MODIS-Landsat time-series data, the optical imagery data are still limited during continuous cloudy and rainy weather, resulting in some uncertainties in our findings. The combination of optical and synthetic aperture radar (SAR) data could enhance the accuracy of identification and the mapping of rice in areas frequently affected by clouds [76]. Thus, future studies could combine optical and SAR time-series data in multi-temporal and large-scale rice mapping studies. Additionally, rice paddies in mountainous areas are generated fragmented, with some fields

being smaller than 30×30 m, making it challenging to accurately identify rice cropping patterns in these areas using newly constructed remote-sensing data. The combined use of Landsat and higher-resolution imagery (e.g., Sentinel-2) may overcome this issue to some extent.

5. Conclusions

We mapped paddy rice cropping patterns with a spatial resolution of 30×30 m over Southern China in 2000 and 2020 by integrating the GF-SG filtering, Eppf-CM, random forest (RF), and the difference in NDVI (DNDVI) method approaches. We found that the rice cropping pattern maps generated for Southern China had high accuracies overall. The planting areas of double-season rice in Southern China decreased by 1244×10^4 hm² during 2000–2020. Compared to the year 2000, the area that shifted from double- to single-season rice in 2020 was 2.71 times larger than that shifting from single- to double-season rice. The decline in the rural labor force, coupled with ≥ 10 °C accumulated temperature and topographical factors, is key to the decrease in rice cropping intensity.

Supplementary Materials: The following supporting information can be downloaded at: <https://www.mdpi.com/article/10.3390/rs16030440/s1>. Figure S1: Temporal profiles of the spectral indices; D1 and D2 denote single-season rice and double-season rice, respectively, Figure S2: Spatial pattern of the change in the planting areas of single-season rice at the county level in southern China during 2000–2020, Figure S3: Comparison between our new rice paddy maps and cropland from GlobeLand30; A–D denote the areas in Yugan County in Jiangxi Province, Xinjian County in Jiangxi Province, Jiuluo County in Hunan Province, and Leizhou County in Guangdong Province, respectively; 1–3 represent the original Sentinel-2 imagery on 12 July 2020, the cropland from GlobeLand30, and the new rice paddy maps, respectively.

Author Contributions: Conceptualization, L.L. and M.D.; methodology, W.Z. and X.P.; investigation, M.Y., X.C., J.C., H.H., Y.D. and J.L.; writing—original draft preparation, W.Z.; writing—review and editing, L.L., M.D., W.L. and Y.L. All authors have read and agreed to the published version of the manuscript.

Funding: This project was financially supported by the National Natural Science Foundation of China (42161021), the Natural Science Foundation of Fujian Province, China (grant no. 2020J05233), and the Xiamen Natural Science Foundation Project (3502ZZ202372044).

Data Availability Statement: Data will be made available on reasonable request. The data are not publicly available due to the data need to be used for further research.

Conflicts of Interest: The authors declare no conflicts of interest.

References

1. FAOSTAT. FAO Statistical Databases (Food and Agriculture Organization of the United Nations) Databases-UW-Madison Libraries. 2020. Available online: <http://digital.library.wisc.edu/1711.web/faostat> (accessed on 16 January 2024).
2. Kuenzer, C.; Knauer, K. Remote sensing of rice crop areas. *Int. J. Remote Sens.* **2013**, *34*, 2101–2139. [[CrossRef](#)]
3. Elert, E. Rice by the numbers: A good grain. *Nature* **2014**, *514*, S50–S51. [[CrossRef](#)] [[PubMed](#)]
4. Godfray, H.C.J.; Beddington, J.R.; Crute, I.R.; Haddad, L.; Lawrence, D.; Muir, J.F.; Pretty, J.; Robinson, S.; Thomas, S.M.; Toulmin, C. Food Security: The Challenge of Feeding 9 Billion People. *Science* **2010**, *327*, 812–818. [[CrossRef](#)]
5. Deng, N.; Grassini, P.; Yang, H.; Huang, J.; Cassman, K.G.; Peng, S. Closing yield gaps for rice self-sufficiency in China. *Nat. Commun.* **2019**, *10*, 1725. [[CrossRef](#)] [[PubMed](#)]
6. Guan, C.; Huang, H.; Huang, G.; Sun, D.; Liang, Y. Problems and Countermeasures of Paddy Field Multiple Cropping in Southern China. *Crops* **2016**, *32*, 1–7.
7. Qiu, B.; Lu, D.; Tang, Z.; Song, D.; Zeng, Y.; Wang, Z.; Chen, C.; Chen, N.; Huang, H.; Xu, W. Mapping cropping intensity trends in China during 1982–2013. *Appl. Geogr.* **2017**, *79*, 212–222. [[CrossRef](#)]
8. Jiang, M.; Xin, L.; Li, X.; Tan, M.; Wang, R. Decreasing Rice Cropping Intensity in Southern China from 1990 to 2015. *Remote Sens.* **2019**, *11*, 35. [[CrossRef](#)]
9. Li, S.; Li, X.; Sun, L.; Cao, G.; Fischer, G.; Tramberend, S. An estimation of the extent of cropland abandonment in mountainous regions of China. *Land Degrad. Dev.* **2018**, *29*, 1327–1342. [[CrossRef](#)]
10. Li, L.; Jiang, P.; Liu, W.; Sun, Y.; Dang, Z. Increasing Spatial Mismatch of Cropland-Grain Production-Population in China over the Past Two Decades. *Land* **2022**, *11*, 1685. [[CrossRef](#)]

11. Liu, L.; Xiao, X.; Qin, Y.; Wang, J.; Xu, X.; Hu, Y.; Qiao, Z. Mapping cropping intensity in China using time series Landsat and Sentinel-2 images and Google Earth Engine. *Remote Sens. Environ.* **2020**, *239*, 111624. [[CrossRef](#)]
12. Weiss, M.; Jacob, F.; Duveiller, G. Remote sensing for agricultural applications: A meta-review. *Remote Sens. Environ.* **2020**, *236*, 111402. [[CrossRef](#)]
13. Zhang, M.; Wu, B.; Zeng, H.; He, G.; Liu, C.; Tao, S.; Zhang, Q.; Nabil, M.; Tian, F.; Bofana, J.; et al. GCI30: A global dataset of 30 m cropping intensity using multisource remote sensing imagery. *Earth Syst. Sci. Data* **2021**, *13*, 4799–4817. [[CrossRef](#)]
14. Kontgis, C.; Schneider, A.; Ozdogan, M. Mapping rice paddy extent and intensification in the Vietnamese Mekong River Delta with dense time stacks of Landsat data. *Remote Sens. Environ.* **2015**, *169*, 255–269. [[CrossRef](#)]
15. Dong, J.; Xiao, X. Evolution of regional to global paddy rice mapping methods: A review. *ISPRS J. Photogramm. Remote Sens.* **2016**, *119*, 214–227. [[CrossRef](#)]
16. Qiu, B.; Hu, X.; Chen, C.; Tang, Z.; Yang, P.; Zhu, X.; Yan, C.; Jian, Z. Maps of cropping patterns in China during 2015–2021. *Sci. Data* **2022**, *9*, 479. [[CrossRef](#)] [[PubMed](#)]
17. Liu, J.; Li, L.; Huang, X.; Liu, Y.; Li, T. Mapping paddy rice in Jiangsu Province, China, based on phenological parameters and a decision tree model. *Front. Earth Sci.* **2019**, *13*, 111–123. [[CrossRef](#)]
18. Zhao, S.; Liu, X.; Ding, C.; Liu, S.; Wu, C.; Wu, L. Mapping Rice Paddies in Complex Landscapes with Convolutional Neural Networks and Phenological Metrics. *Gisci. Remote Sens.* **2020**, *57*, 37–48. [[CrossRef](#)]
19. Ding, M.; Chen, Q.; Xin, L.; Li, L.; Xiubin, L.I.; Bai, W. Spatial and temporal variations of multiple cropping index in China based on SPOT-NDVI during 1999–2013. *Acta Geogr. Sin.* **2015**, *70*, 1080–1090.
20. Qiu, B.; Qi, W.; Tang, Z.; Chen, C.; Wang, X. Rice cropping density and intensity lessened in southeast China during the twenty-first century. *Environ. Monit. Assess.* **2016**, *188*, 5. [[CrossRef](#)]
21. Jain, M.; Mondal, P.; DeFries, R.S.; Small, C.; Galford, G.L. Mapping cropping intensity of smallholder farms: A comparison of methods using multiple sensors. *Remote Sens. Environ.* **2013**, *134*, 210–223. [[CrossRef](#)]
22. He, Y.; Dong, J.; Liao, X.; Sun, L.; Wang, Z.; You, N.; Li, Z.; Fu, P. Examining rice distribution and cropping intensity in a mixed single- and double-cropping region in South China using all available Sentinel 1/2 images. *Int. J. Appl. Earth Obs. Geoinf.* **2021**, *101*, 102351. [[CrossRef](#)]
23. Pan, B.; Zheng, Y.; Shen, R.; Ye, T.; Zhao, W.; Dong, J.; Ma, H.; Yuan, W. High Resolution Distribution Dataset of Double-Season Paddy Rice in China. *Remote Sens.* **2021**, *13*, 4609. [[CrossRef](#)]
24. Tian, H.; Wu, M.; Wang, L.; Niu, Z. Mapping Early, Middle and Late Rice Extent Using Sentinel-1A and Landsat-8 Data in the Poyang Lake Plain, China. *Sensors* **2018**, *18*, 185. [[CrossRef](#)]
25. Gao, F.; Anderson, M.C.; Zhang, X.; Yang, Z.; Alfieri, J.G.; Kustas, W.P.; Mueller, R.; Johnson, D.M.; Prueger, J.H. Toward mapping crop progress at field scales through fusion of Landsat and MODIS imagery. *Remote Sens. Environ.* **2017**, *188*, 9–25. [[CrossRef](#)]
26. Zhu, X.; Chen, J.; Gao, F.; Chen, X.; Masek, J.G. An enhanced spatial and temporal adaptive reflectance fusion model for complex heterogeneous regions. *Remote Sens. Environ.* **2010**, *114*, 2610–2623. [[CrossRef](#)]
27. Chen, Y.; Cao, R.; Chen, J.; Liu, L.; Matsushita, B. A practical approach to reconstruct high-quality Landsat NDVI time-series data by gap filling and the Savitzky–Golay filter. *ISPRS J. Photogramm. Remote Sens.* **2021**, *180*, 174–190. [[CrossRef](#)]
28. Cao, R.; Xu, Z.; Chen, Y.; Chen, J.; Shen, M. Reconstructing High-Spatiotemporal-Resolution (30 m and 8-Days) NDVI Time-Series Data for the Qinghai–Tibetan Plateau from 2000–2020. *Remote Sens.* **2022**, *14*, 3648. [[CrossRef](#)]
29. Ma, Y.; Lyu, D.; Sun, K.; Li, S.; Zhu, B.; Zhao, R.; Zheng, M.; Song, K. Spatiotemporal Analysis and War Impact Assessment of Agricultural Land in Ukraine Using RS and GIS Technology. *Land* **2022**, *11*, 1810. [[CrossRef](#)]
30. Ding, M.; Guan, Q.; Li, L.; Zhang, H.; Liu, C.; Zhang, L. Phenology-Based Rice Paddy Mapping Using Multi-Source Satellite Imagery and a Fusion Algorithm Applied to the Poyang Lake Plain, Southern China. *Remote Sens.* **2020**, *12*, 1022. [[CrossRef](#)]
31. Yin, Q.; Liu, M.; Cheng, J.; Ke, Y.; Chen, X. Mapping Paddy Rice Planting Area in Northeastern China Using Spatiotemporal Data Fusion and Phenology-Based Method. *Remote Sens.* **2019**, *11*, 1699. [[CrossRef](#)]
32. Xiao, X.; Boles, S.; Liu, J.; Zhuang, D.; Frolking, S.; Li, C.; Salas, W.; Moore, B. Mapping paddy rice agriculture in southern China using multi-temporal MODIS images. *Remote Sens. Environ.* **2005**, *95*, 480–492. [[CrossRef](#)]
33. Dong, J.; Xiao, X.; Kou, W.; Qin, Y.; Zhang, G.; Li, L.; Jin, C.; Zhou, Y.; Wang, J.; Biradar, C.; et al. Tracking the dynamics of paddy rice planting area in 1986–2010 through time series Landsat images and phenology-based algorithms. *Remote Sens. Environ.* **2015**, *160*, 99–113. [[CrossRef](#)]
34. Zhang, G.; Xiao, X.; Biradar, C.M.; Dong, J.; Qin, Y.; Menarguez, M.A.; Zhou, Y.; Zhang, Y.; Jin, C.; Wang, J.; et al. Spatiotemporal patterns of paddy rice croplands in China and India from 2000 to 2015. *Sci. Total Environ.* **2017**, *579*, 82–92. [[CrossRef](#)] [[PubMed](#)]
35. You, N.; Dong, J. Examining earliest identifiable timing of crops using all available Sentinel 1/2 imagery and Google Earth Engine. *ISPRS J. Photogramm. Remote Sens.* **2020**, *161*, 109–123. [[CrossRef](#)]
36. Ni, R.; Tian, J.; Li, X.; Yin, D.; Li, J.; Gong, H.; Zhang, J.; Zhu, L.; Wu, D. An enhanced pixel-based phenological feature for accurate paddy rice mapping with Sentinel-2 imagery in Google Earth Engine. *ISPRS J. Photogramm. Remote Sens.* **2021**, *178*, 282–296. [[CrossRef](#)]
37. Yan, H.; Liu, F.; Qin, Y. Tracking the spatio-temporal change of cropping intensity in China during 2000–2015. *Environ. Res. Lett.* **2019**, *14*, 35008. [[CrossRef](#)]
38. Qiu, B.; Yan, C.; Huang, W. Progress and Prospect on Mapping Cropping Systems Using Time Series Images. *J. Geo-Inf. Sci.* **2022**, *1*, 176–188.

39. Peng, D.; Huete, A.R.; Huang, J.; Wang, F.; Sun, H. Detection and estimation of mixed paddy rice cropping patterns with MODIS data. *Int. J. Appl. Earth Obs. Geoinf.* **2011**, *13*, 13–23. [[CrossRef](#)]
40. Li, W. *Research on the Spatio-Temporal Pattern and Change of Rice Cropping Systems in the Middle Reaches of Yangtze River*; University of Chinese Academy of Sciences: Beijing, China, 2015; Volume D.
41. Li, P.; Feng, Z.; Jiang, L.; Liu, Y.; Xiao, X. Changes in rice cropping systems in the Poyang Lake Region, China during 2004–2010. *J. Geogr. Sci.* **2012**, *22*, 653–668. [[CrossRef](#)]
42. Zhong, F.; Lu, W.; Xu, Z. Is the Outmigration of Rural Labor Force Detrimental to Grain Production?—Analysis of Farmers’ Factor Substitution and Cropping Structure Adjustment Behavior and Its Constraints. *Chin. Rural. Econ.* **2016**, *7*, 36–47.
43. Xie, H.; Liu, G. Spatiotemporal differences and influencing factors of multiple cropping index in China during 1998–2012. *J. Geogr. Sci.* **2015**, *25*, 1283–1297. [[CrossRef](#)]
44. Frolking, S.; Qiu, J.; Boles, S.; Xiao, X.; Liu, J.; Zhuang, Y.; Li, C.; Qin, X. Combining remote sensing and ground census data to develop new maps of the distribution of rice agriculture in China. *Glob. Biogeochem. Cycles* **2002**, *16*, 31–38. [[CrossRef](#)]
45. Liu, T.; Peng, R.; Zhuo, Y.; Cao, G. China’s changing population distribution and influencing factors: Insights from the 2020 census data. *Acta Geogr. Sin.* **2022**, *77*, 381–394.
46. Deng, F.; Cao, L.; Li, F.; Li, L.; Man, W.; Chen, Y.; Liu, W.; Peng, C. Mapping China’s Changing Gross Domestic Product Distribution Using Remotely Sensed and Point-of-Interest Data with Geographical Random Forest Model. *Sustainability* **2023**, *15*, 8062. [[CrossRef](#)]
47. Dong, J.; Wu, W.; Huang, J.; You, N.; He, Y.; Yan, H. State of the Art and Perspective of Agricultural Land Use Remote Sensing Information Extraction. *J. Geo-Inf. Sci.* **2020**, *22*, 772–783.
48. Jin, Q.; Xu, E.; Zhang, X. A Fusion Method for Multisource Land Cover Products Based on Superpixels and Statistical Extraction for Enhancing Resolution and Improving Accuracy. *Remote Sens.* **2022**, *14*, 1676. [[CrossRef](#)]
49. Chen, J.; Ban, Y.; Li, S. Open access to Earth land-cover map. *Nature* **2014**, *523*, 434.
50. Zhang, X.; Liu, L.; Chen, X.; Gao, Y.; Xie, S.; Mi, J. GLC_FCS30: Global land-cover product with fine classification system at 30 m using time-series Landsat imagery. *Earth Syst. Sci. Data* **2021**, *13*, 2753–2776. [[CrossRef](#)]
51. Kuang, W.; Liu, J.; Tian, H.; Shi, H.; Dong, J.; Song, C.; Li, X.; Du, G.; Hou, Y.; Lu, D.; et al. Cropland redistribution to marginal lands undermines environmental sustainability. *Natl. Sci. Rev.* **2022**, *9*, nwab091. [[CrossRef](#)]
52. Yang, J.; Huang, X. The 30 m annual land cover dataset and its dynamics in China from 1990 to 2019. *Earth Syst. Sci. Data* **2021**, *13*, 3907–3925. [[CrossRef](#)]
53. Sun, C.; Zhang, H.; Xu, L.; Ge, J.; Jiang, J.; Zuo, L.; Wang, C. Twenty-meter annual paddy rice area map for mainland Southeast Asia using Sentinel-1 synthetic-aperture-radar data. *Earth Syst. Sci. Data* **2023**, *15*, 1501–1520. [[CrossRef](#)]
54. Qiu, B.; Jiang, F.; Chen, C.; Tang, Z.; Wu, W.; Berry, J. Phenology-pigment based automated peanut mapping using sentinel-2 images. *Gisci. Remote Sens.* **2021**, *58*, 1335–1351. [[CrossRef](#)]
55. Bera, B.; Saha, S.; Bhattacharjee, S. Estimation of Forest Canopy Cover and Forest Fragmentation Mapping Using Landsat Satellite Data of Silabati River Basin (India). *KN-J. Cartogr. Geogr. Inf.* **2020**, *70*, 181–197. [[CrossRef](#)]
56. Xiao, X.; Hollinger, D.; Aber, J.; Goltz, M.; Davidson, E.A.; Zhang, Q.; Moore, B. Satellite-based modeling of gross primary production in an evergreen needleleaf forest. *Remote Sens. Environ.* **2004**, *89*, 519–534. [[CrossRef](#)]
57. Gitelson, A.A.; Gritz, Y.; Merzlyak, M.N. Relationships between leaf chlorophyll content and spectral reflectance and algorithms for non-destructive chlorophyll assessment in higher plant leaves. *J. Plant Physiol.* **2003**, *160*, 271–282. [[CrossRef](#)] [[PubMed](#)]
58. Tucker, C.J. Red and photographic infrared linear combinations for monitoring vegetation. *Remote Sens. Environ.* **1979**, *8*, 127–150. [[CrossRef](#)]
59. Huete, A.; Didan, K.; Miura, T.; Rodriguez, E.P.; Gao, X.; Ferreira, L.G. Overview of the radiometric and biophysical performance of the MODIS vegetation indices. *Remote Sens. Environ.* **2002**, *83*, 195–213. [[CrossRef](#)]
60. Merzlyak, M.N.; Gitelson, A.A.; Chivkunova, O.B.; Rakitin, V.Y. Non-destructive optical detection of pigment changes during leaf senescence and fruit ripening. *Physiol. Plant.* **1999**, *106*, 135–141. [[CrossRef](#)]
61. Zhang, T.; Yang, X.; Wang, H.; Li, Y.; Ye, Q. Climatic and technological ceilings for Chinese rice stagnation based on yield gaps and yield trend pattern analysis. *Glob. Change Biol.* **2014**, *20*, 1289–1298. [[CrossRef](#)]
62. Breiman, L. Random forests. *Mach. Learn.* **2001**, *45*, 5–32. [[CrossRef](#)]
63. Belgiu, M.; Drăguț, L. Random forest in remote sensing: A review of applications and future directions. *ISPRS J. Photogramm. Remote Sens.* **2016**, *114*, 24–31. [[CrossRef](#)]
64. Chen, A.; Li, Y. Rice recognition of different growth stages based on Sentinel-2 images in mountainous areas of Southwest China. *Trans. Chin. Soc. Agric. Eng.* **2020**, *36*, 192–199.
65. Li, Y.; Zhang, L.; Yan, J.; Wang, P.; Hu, N.; Cheng, W.; Fu, B. Mapping the hotspots and coldspots of ecosystem services in conservation priority setting. *J. Geogr. Sci.* **2017**, *27*, 681–696. [[CrossRef](#)]
66. Wang, J.F.; Li, X.H.; Christakos, G.; Liao, Y.L.; Zhang, T.; Gu, X.; Zheng, X.Y. Geographical Detectors-Based Health Risk Assessment and its Application in the Neural Tube Defects Study of the Heshun Region, China. *Int. J. Geogr. Inf. Sci.* **2010**, *24*, 107–127. [[CrossRef](#)]
67. Song, Y.; Wang, J.; Ge, Y.; Xu, C. An optimal parameters-based geographical detector model enhances geographic characteristics of explanatory variables for spatial heterogeneity analysis: Cases with different types of spatial data. *Gisci. Remote Sens.* **2020**, *57*, 593–610. [[CrossRef](#)]

68. Xu, C.; Li, Y.; Wang, J.; Xiao, G. Spatial-temporal detection of risk factors for bacillary dysentery in Beijing, Tianjin and Hebei, China. *BMC Public Health* **2017**, *17*, 743. [[CrossRef](#)] [[PubMed](#)]
69. Song, Q.; Hu, Q.; Zhou, Q.; Hovis, C.; Xiang, M.; Tang, H.; Wu, W. In-Season Crop Mapping with GF-1/WFV Data by Combining Object-Based Image Analysis and Random Forest. *Remote Sens.* **2017**, *9*, 1184. [[CrossRef](#)]
70. Huang, C.; You, S.; Liu, A.; Li, P.; Zhang, J.; Deng, J. High-Resolution National-Scale Mapping of Paddy Rice Based on Sentinel-1/2 Data. *Remote Sens.* **2023**, *15*, 4055. [[CrossRef](#)]
71. Gan, C.; Qiu, B.; Zhang, J.; Yao, C.; Ye, Z.; Huang, G.; Huang, Y.; Peng, Y.; Lin, Y.; Lin, D.; et al. Mapping paddy rice planting patterns based on Sentinel-1/2. *J. Geo-Inf. Sci.* **2023**, *25*, 153–162.
72. Zhang, J.; Lliu, Y.; Zhang, E.; Chen, J.; Tan, Q.; Acharya Nalan, S. Dynamics and driving mechanisms of cultivated land at county level in China. *Acta Geogr. Sin.* **2023**, *78*, 2105–2127.
73. Dong, S.; Xin, L.; Li, S.; Xie, H.; Yuluan, Z.; Xue, W.; Xiubin, L.I.; Hengfei, S.; Yahan, L.U.; Acharya Nalan, S. The extent and spatial distribution of terrace abandonment in China. *Acta Geogr. Sin.* **2023**, *78*, 3–15. [[CrossRef](#)]
74. Xie, H.; Wu, Q.; Li, X. Impact of labor transfer differences on terrace abandonment: Evidence from micro-survey of farmers in the mountainous areas of Hunan, Fujian and Jiangxi. *Acta Geogr. Sin.* **2023**, *78*, 16–34.
75. Li, Y.; Qiu, B.; He, Y.; Chen, G.; Ye, Z. Crop intensity based on MODIS data in China during 2001–2018. *Prog. Geogr. Sci.* **2020**, *39*, 1874–1883. [[CrossRef](#)]
76. Mansaray, L.R.; Yang, L.; Kabba, V.T.S.; Kanu, A.S.; Huang, J.; Wang, F. Optimising rice mapping in cloud-prone environments by combining quad-source optical with Sentinel-1A microwave satellite imagery. *Gisci. Remote Sens.* **2019**, *56*, 1333–1354. [[CrossRef](#)]

Disclaimer/Publisher’s Note: The statements, opinions and data contained in all publications are solely those of the individual author(s) and contributor(s) and not of MDPI and/or the editor(s). MDPI and/or the editor(s) disclaim responsibility for any injury to people or property resulting from any ideas, methods, instructions or products referred to in the content.